

# Digital Filters for Reducing Background Noise in Micro PIV Measurements

by

L. Gui<sup>(1)</sup>, S. T. Wereley<sup>(2)</sup> and S.Y. Lee<sup>(3)</sup>

Mechanical Engineering, Purdue University West Lafayette, IN 47907-1288

E-Mail: <sup>(1)</sup>[gui@purdue.edu](mailto:gui@purdue.edu), <sup>(2)</sup>[wereley@purdue.edu](mailto:wereley@purdue.edu) and <sup>(3)</sup>[leesy1@ecn.purdue.edu](mailto:leesy1@ecn.purdue.edu)

## ABSTRACT

In the present work digital filters are used to reduce the measurement uncertainty of the microscopic particle image velocimetry ( $\mu$ PIV) technique. Analysis shows that single pixel random noise and low frequency background noise in the  $\mu$ PIV recordings are much stronger than in the usual macroscopic PIV recordings. The effects of several different low- and high-pass filters on the evaluation accuracy of a correlation-based interrogation algorithm with continuous window shift and central difference image correction are investigated. Simulations show that the  $3 \times 3$ -pixel rectangular smooth filter can reduce effectively the evaluation error resulting from single pixel random noise. The unsharp mask is a powerful tool to reduce the evaluation error caused by low frequency background noise. A  $\mu$ PIV image filter that combines the capabilities of both the smooth filter and the unsharp mask is constructed to enable high accuracy evaluation of  $\mu$ PIV recordings.

The  $\mu$ PIV image filter is applied in the PIV experiment of water flow in a deep microchannel of  $200\mu\text{m} \times 600\mu\text{m} \times 120\text{mm}$ . As shown in in Fig. 7, the  $\mu$ PIV recordings have a strong single pixel random noise level and low frequency noises of different wavelengths. Averaged correlation functions are given in Fig.8a and 8b, respectively, for the cases with and without using  $\mu$ PIV image filter. Fig.8a shows that in the case without filtering the low frequency noise results in a dominant peak in the evaluation function at zero displacement. The correlation peak of the particle image displacement can not be identified in the presence of this noise peak. When the  $\mu$ PIV image filter is used to remove the low frequency noise, a clear peak of the particle image displacement is observed, see Fig.8b. The axial velocity ( $U$ ) profile of the fully developed microchannel flow is and shown in Fig.9a. The distributions of the standard deviation ( $\sigma$ ) of the axial velocity are provided in Fig.9b. The test results show that a much lower precision error level can be achieved by using  $\mu$ PIV image filter.

## Abbreviations

CCWS	correlation-based interrogation algorithm with continuous window shift
CDIC	central difference image correction
FFT	fast Fourier transformation
$\mu$ PIV	micro particle image velocimetry
PIV	particle image velocimetry
RMS	root-mean-square
RSS	root-sum-square

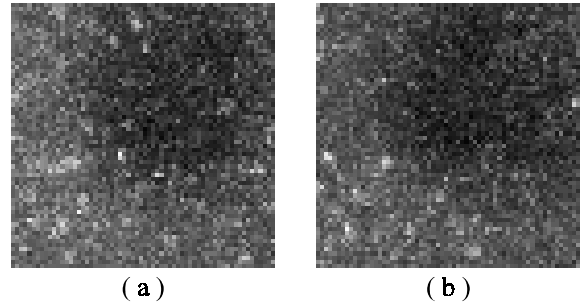


Fig.7:  $\mu$ PIV evaluation sample pair (64 $\times$ 64 pixels)

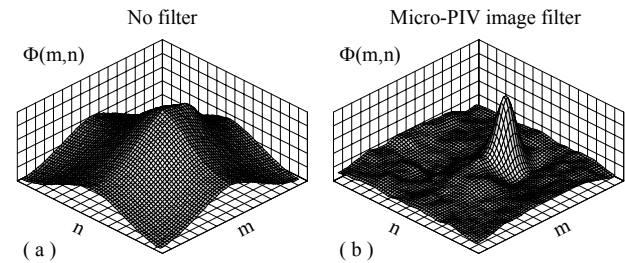


Fig.8: Correlation funcs: (a) No filter, (b) Using  $\mu$ PIV image filter.

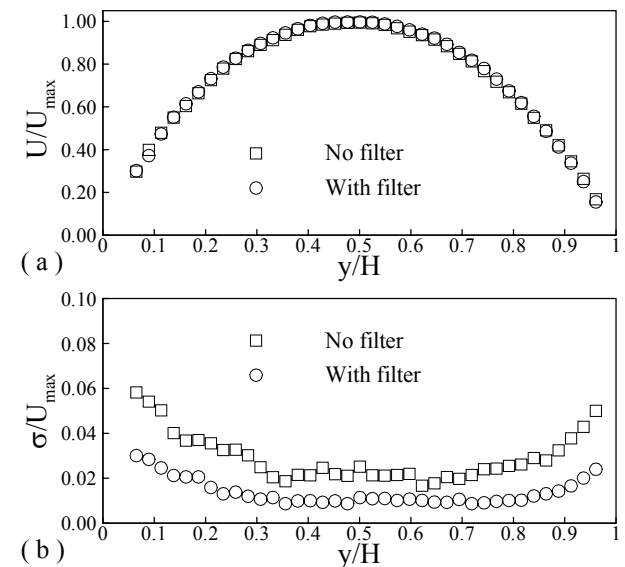


Fig. 9: Velocity profile (a) measured using  $\mu$ PIV in a microchannel and the standard deviation (b) of the measurement results

## 1. INTRODUCTION

Micro particle image velocimetry is becoming a general tool for investigating flows in micro-scale devices. Santiago, et al. (1998) described the first  $\mu$ PIV system consisting of an epi-fluorescent microscope, an intensified CCD camera and a continuous Hg-arc lamp capable of measuring slow flows in micro devices with a spatial resolution of  $6.9 \times 6.9 \times 1.5 \mu\text{m}^3$ .  $\mu$ PIV was used to measure slow flows around a red blood cell with a spatial resolution of  $3.5 \times 3.5 \mu\text{m}^2$  (Wereley et al. 1998). Later applications of the  $\mu$ PIV technique moved steadily toward faster flows by replacing the continuous Hg-arc lamp with a two-headed Nd:YAG laser and an interline transfer camera, with which singly-exposed PIV recording pairs can be acquired with a sub-microsecond time interval (Meinhart et al., 1999; Meinhart and Zhang, 2000). Wereley et al. (2002) reviewed  $\mu$ PIV details and recent advances in the technique. Currently, volume illumination, small particles and Brownian motion are three fundamental problems that differentiate  $\mu$ PIV from conventional macroscopic PIV. The first two of these problems reduce the contrast between  $\mu$ PIV particle images and the background to levels significantly lower than that for macroscopic PIV. Generally, the image quality of  $\mu$ PIV recordings is much lower than that of macroscopic PIV recordings, and the  $\mu$ PIV recordings usually have a low image density.

The correlation-based interrogation and tracking algorithms are usually used to evaluate the  $\mu$ PIV recordings. The correlation-based interrogation algorithm has played a major role in evaluating PIV recordings since the first application of the digital PIV technique. It correlates the gray value distributions in two equal-sized interrogation windows, one chosen from each of the two digital images comprising a PIV recording pair. The correlation computation is usually accelerated with the fast Fourier transformation (FFT) algorithm. Details of the correlation-based interrogation algorithm were described, discussed, and reviewed by Cenedese and Paglialunga (1990), Keane and Adrian (1990), Adrian (1991), Willert and Gharib (1991), Heckmann et al. (1994), and Westerweel et al. (1996). Using the FFT algorithm brings several problems to the correlation-based interrogation algorithm, such as large evaluation errors at large particle image displacements and large bias gradient around zero displacement, which increase the measurement uncertainties of the mean velocities and Reynolds stresses, respectively, in turbulent flow measurements (Gui et al. 2001). In order to avoid the large evaluation errors at large particle image displacements, a discrete window shift is often applied (Willert 1996; Westerweel et al. 1997). For reducing the bias error and bias gradient around the zero displacement, a Gaussian window mask is adopted (Gui et al. 2000, 2001). The correlation function has also been used as a tracking criterion for determining the displacement of an image pattern that contains a group of particle images. Correlation-based tracking schemes were described and applied by Huang et al. (1993), Kemmerich and Rath (1994), Okamoto et al. (1995), and Fincham and Spedding (1997). When using a correlation-based tracking algorithm, the first interrogation window defines the particle image pattern to be tracked, while the second interrogation window determines the tracking area, so that the second interrogation window is larger than the first. In comparison with the original correlation-based interrogation, the correlation-based tracking achieves a higher accuracy at large particle image displacements and avoids the large bias error and bias gradient around zero displacement, so that it was considered to be a better algorithm for a long time period. However, a multi-pass continuous window shift technique largely increases the evaluation accuracy of the correlation-based interrogation scheme (Sjödahl, 1994; Sholl et al., 1997; Lecordier et al., 1999, 2001). An evaluation conducted by Gui and Wereley (2002) indicated that when combined with the continuous window shift technique the correlation-based interrogation algorithm exhibits much better performance than the correlation-based tracking algorithm. Further advances of the evaluation algorithm are the central difference interrogation (Wereley et al., 1998; Wereley and Meinhart, 2000, 2001) and particle image pattern correction (Huang et al., 1993; Tokumaru and Dimotakis, 1995; Fincham and Spedding, 1997; Lin and Perlin, 1998; Nogueira et al, 1999, 2001; Scarano, 2002). Recently, Wereley and Gui (2001, 2002) described a central difference image correction (CDIC) method that combines ideas of central difference interrogation, adaptive continuous window shift and particle image pattern correction, enabling a very reliable and accurate evaluation of digital PIV recordings in a wide variety of circumstances. In order to increase the signal-to-noise ratio of the  $\mu$ PIV recordings, Meinhart, et al. (2000) developed an average correlation method that is widely used in the evaluation of  $\mu$ PIV recordings.

Digital filters are basic tools for improving the quality of digital images. They are described in many books related to digital signal and image processing, e.g. Lim JS (1990). In general, low-pass filters can be used to reduce the high frequency noise sources in digital images, whereas high-pass filters can be used to minimize the low-frequency noise. Many researchers tried to apply the digital filters to increase the measurement accuracy of PIV, e.g. Mass (1992), Heckmann (1996) and Gui (1998). However, improper use of digital filters in PIV recording evaluation may cause serious problems. For instance, the high-pass filter may strengthen random noise sources and low-pass filters may eliminate the fine structures of particle images. In the present work, the effects of several different digital filters on the evaluation accuracy of  $\mu$ PIV recordings by using the correlation-based interrogation with continuous window shift and image correction are investigated. A new digital filter is constructed to enable a high accuracy evaluation of  $\mu$ PIV recordings and applied in PIV tests conducted in a microchannel.

## 2. PIV IMAGE AND BACKGROUND NOISE

When the tracer particles illuminated by the laser are small enough to be considered as point light sources, they have an intensity distribution given by the Airy function, which is reasonably well approximated by a Gaussian function. The Gaussian distribution of a particle image intensity (gray value) in the image plane  $(x,y)$  can be described by

$$G_p(x,y) = G_c \exp\left(-2 \frac{(x-x_0)^2 + (y-y_0)^2}{D_p^2}\right) \quad (1)$$

where  $D_p$ ,  $G_c$  and  $(x_0,y_0)$  are diameter, center brightness and position of the particle image, respectively. The traditional macroscopic PIV technique usually requires the particle image diameter to be around 1.5 pixels to achieve the maximal accuracy of the correlation-based interrogation algorithm. However, particle images in  $\mu$ PIV recordings are usually much larger, i.e.  $D_p=3\sim 6$  pixels. Usually, the Airy or Gaussian distributions of particle images can hardly be identified in  $\mu$ PIV recordings because of strong background noise sources.

The most frequently observed noise in  $\mu$ PIV recordings results from thermal noise in the CCD array. Since this noise is related to individual pixels and has a random intensity distribution, we refer it to as single pixel random noise. The single pixel random noise ( $G_{sp}$ ) includes a constant portion  $G_o$  and a random portion  $G_r$ , i.e.

$$G_{sp}(x,y) = G_o + G_r(x,y) \quad (2)$$

$G_r$  has a Gaussian probability distribution in the  $\mu$ PIV recording and can be quantified with the root-mean-square (RMS) value

$$G_{rms} = \sqrt{\frac{1}{MN} \sum_{x=1}^M \sum_{y=1}^N G_r^2(x,y)} \quad (3)$$

where  $M$  and  $N$  are width and height of the digital PIV recording, respectively. In the following we refer  $G_{rms}$  to the intensity of single pixel random noise. As an example, the probability distribution function of gray value in a digital PIV recording taken in a micro channel is given in Fig.1 in form of a histogram. An image sample of  $32 \times 32$  pixels is also shown in this figure. The histogram has a Gaussian peak centered at 41 that indicates the mean gray value of the background. The standard deviation of the gray values around the mean ( $\approx G_{rms}$ ) is 8. The gray level of the particles in this  $\mu$ PIV recording is around 150.

Another kind of background noise results from non-uniform illumination, particle clusters out of the focal plane, unexpected reflection etc. It has a relatively low spatial frequency, and in many cases, it is unchanged from frame to frame. In order to investigate its influence on the evaluation accuracy of the  $\mu$ PIV recordings, the following function is used to simulate the low frequency background noise:

$$G_{lf}(x,y) = A_{lf} \sin\left(\frac{2\pi \cdot x}{\lambda_x} + \phi\right) \cdot \sin\left(\frac{2\pi \cdot y}{\lambda_y} + \varphi\right) \quad (4)$$

Wherein  $A_{lf}$  is the amplitude of the low frequency background noise;  $\lambda_x$  and  $\lambda_y$  are the wavelength in x- and y-direction, respectively;  $\phi$  and  $\varphi$  are the initial phases.

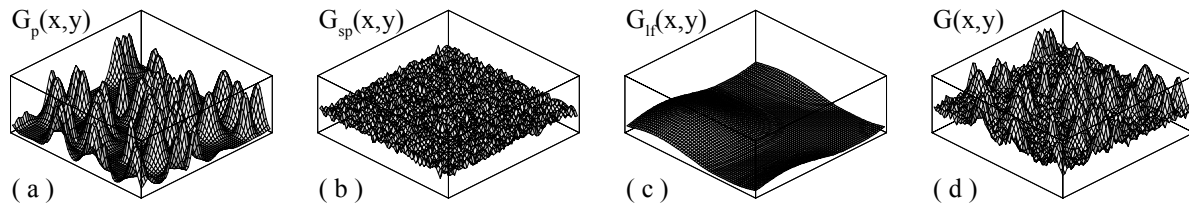


**Fig. 2:** Components of intensity distribution in  $\mu$ PIV recording

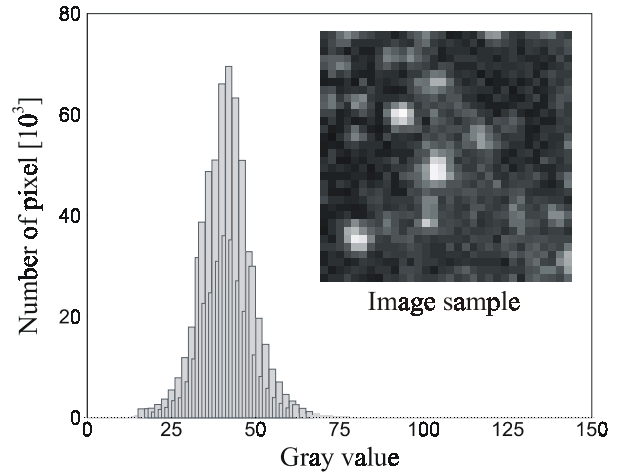


**Fig.1:** Histogram of a micro-PIV recording

As illuminated in Fig.2, the total gray value distribution of the  $\mu$ PIV recording ( $G$ ) is considered as a root-sum-square (RSS) of the Gaussian particle images ( $G_p$ ), the single pixel random noise ( $G_{sp}$ ), and the low frequency background noise ( $G_{lf}$ ), i.e.

$$G(x, y) = \sqrt{G_p^2 + G_{sp}^2 + G_{lf}^2} \quad (5)$$

Most of following discussions are based on synthetically generated PIV recording pairs of size of  $1024 \times 1024$  pixels. The total particle number  $N_{tot}$  is given to determine the particle image number density. The particle position  $(x_0, y_0)$  are determined by a random number generator with uniform probability distribution in the image plane. The particle image brightness and diameter,  $G_c$  and  $D_p$  are also randomly determined in some of the simulations by a similar procedure.  $G_\theta$  is given to determine the mean value of the single pixel random noise.  $G_r(x, y)$  has a Gaussian probability distribution that is determined by a given  $G_{rms}$ . The low frequency background noise is generated with equation (4). A four-roll-mill flow (Wereley and Gui 2001) is simulated by synthetic PIV recording pairs with zero displacement in the center and 0.52 pixels at the four corners, so that the particle image displacements evaluated with a  $16 \times 16$ -pixel grid structure have an uniform distribution between  $-0.5$  and  $0.5$  pixels.

### 3. $\mu$ PIV IMAGE FILTERING

#### 3.1. Digital filters

The simplest kind of digital filter is the linear homogeneous filter defined by

$$G'(x, y) = \sum_{-r}^r \sum_{-r}^r C(i, j) \cdot G(x - i, y - j) \quad (6)$$

where  $C(i, j)$  is the coefficient of the filter mask of size of  $(2r+1) \times (2r+1)$ ;  $G$  and  $G'$  are the gray value distribution of the digital image before and after filtering, respectively. With different filter masks, different low- and high-pass filters are constructed in the linear homogeneous filter family. The simplest low-pass filter is the rectangular smooth filter determined by filter mask

$$C(i, j) = \frac{1}{(2r+1) \cdot (2r+1)} \quad \text{for } -r \leq i \leq r \text{ and } -r \leq j \leq r. \quad (7)$$

Examples of simple high-pass filters are

$$\text{Gradient filter: } C = \frac{1}{2} \begin{bmatrix} 0 & -1 & 0 \\ -1 & 2 & 0 \\ 0 & 0 & 0 \end{bmatrix}, \quad (8)$$

$$\text{Laplace filter: } C = \frac{1}{4} \begin{bmatrix} 0 & -1 & 0 \\ -1 & 4 & -1 \\ 0 & -1 & 0 \end{bmatrix}. \quad (9)$$

The gradient filter is one of several filters that conduct the first order differential operation. The Laplace filter conducts the second order differential operation. A more complicated high-pass filter, i.e. the unsharp mask, has been applied to digital PIV recordings by some researchers to remove the low frequency background noise. It is defined as

$$G'(x, y) = G(x, y) - \frac{1}{(2r+1) \cdot (2r+1)} \sum_{-r}^r \sum_{-r}^r G(x - i, y - j) \quad (10)$$

The size of the unsharp mask should be determined according to the spatial frequencies of particle images and noises.

### 3.2. Effects of digital filters on PIV recording evaluation

Our investigation begins with tests of the 3×3-pixel smooth filter, gradient filter and Laplace filter using synthetic PIV recording pairs with ideal Gaussian particle images, i.e. without any noise. 14 synthetic PIV recording pairs are generated with total particle number  $N_{tot}=20480$ , brightness  $G_c=250$  and particle image diameters  $D_p=0.5\sim 6$  pixels. These synthetic PIV recording pairs are processed with the three different digital filters, respectively, and then evaluated using the CCWS method. A 16×16-pixel evaluation grid structure and a 32×32-pixel interrogation window are used in the evaluation. The RMS evaluation errors for different particle image diameters and different digital filters are given in Fig. 3. The test results show that the gradient filter and Laplace filter can only reduce the evaluation error when the particle image diameter is larger than 5 pixels, otherwise they increase the evaluation error. The 3×3-pixel smooth filter effectively reduces the evaluation error at small particle diameters but increases the evaluation error at large particle diameters. The minimal evaluation errors in the cases with and without the smooth filter are almost the same, and it seems that the smooth filter shifts the minimal point of the evaluation error distribution from 3 pixels to 1.5 pixels.

The smooth filter is further tested with synthetic PIV recording pairs that include the single pixel random noise. 8 pairs of synthetic PIV recordings are generated with different noise intensities. In these synthetic PIV recording pairs the parameters are set as  $N_{tot}=10240$ ,  $G_0=90$ ,  $G_c=180$ , and  $D_p=3\sim 6$  pixels (i.e. particle image size range of most current  $\mu$ PIV recordings). These synthetic PIV recording pairs are processed with the rectangular smooth filter of four different mask sizes respectively and then evaluated using CCWS with a 32×32-pixel interrogation window. The evaluation error dependence on the noise intensity is shown in Fig. 4. The evaluation errors without filtering are also given in the figure for comparison. The test results indicate that the 3×3-pixel smooth filter effectively reduces the evaluation error at high noise intensity, ( $G_{rms}/G_c>0.1$ ), and it just slightly increases the evaluation error at low random noise intensity. The smooth filters of larger mask size generally increase the evaluation error, except for the 5×5-pixel

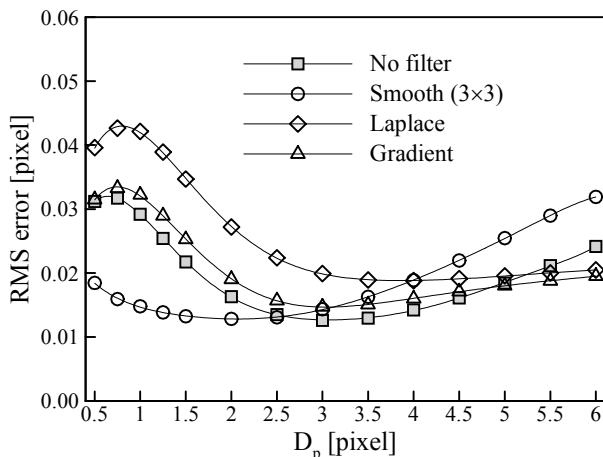


Fig.3: Evaluation error of for ideal particle images processed with different filters

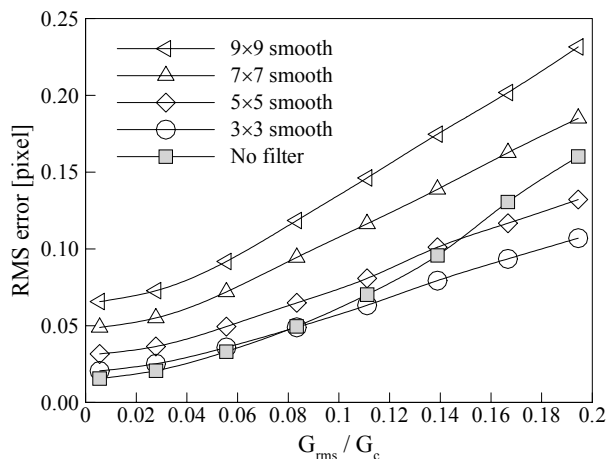


Fig.4: Evaluation error distributions on the random noise intensity for different smooth filters

smooth filter effectively reduces the evaluation error at high noise intensity, ( $G_{rms}/G_c>0.1$ ), and it just slightly increases the evaluation error at low random noise intensity. The smooth filters of larger mask size generally increase the evaluation error, except for the 5×5-pixel

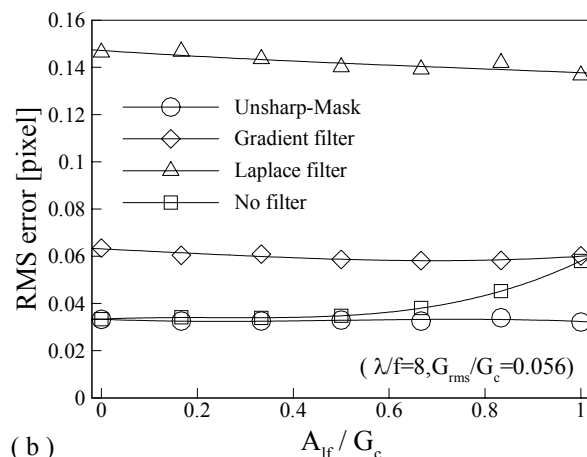
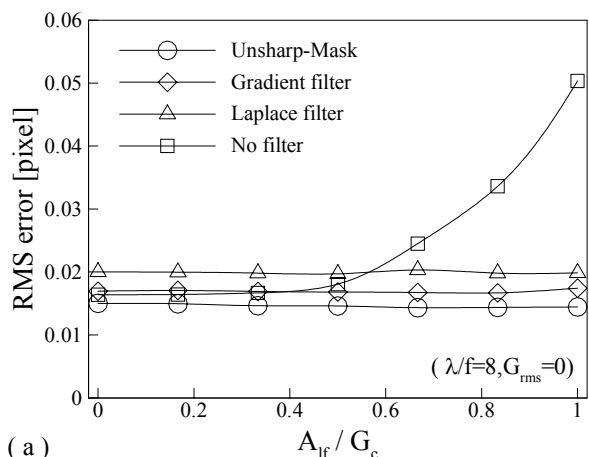


Fig. 5: Test results of three different high-pass filters using synthetic PIV recording pairs with low frequency noise: (a) No random noise, (b) With random noise

smooth filter in the region of  $G_{rms}/G_c > 0.15$ . Additional investigations show that the influence of the mean noise value  $G_0$  on the evaluation uncertainty is very small in comparison with that of the random noise intensity  $G_{rms}$ .

The effects of high-pass filters are investigated using synthetic PIV recording pairs with low frequency background noise. The particle image parameters are set as  $N_{tot}=20480$ ,  $G_0=90$ ,  $G_c=180$ , and  $D_p=3\sim 6$  pixels. The simulated low frequency background noise has a wavelength of 512 pixels, and its amplitude varies in the region of  $A_{lf}/G_c=0\sim 1$ . The investigation is conducted with two steps: in the first step there is no single pixel random noise, whereas in the second step single pixel random noise of  $G_{rms}/G_c=0.056$  is added. These synthetic PIV recording pairs are processed with the gradient filter, Laplace filter and  $21\times 21$ -pixel ( $r=10$ ) unsharp mask, respectively, and then evaluated using the CCWS algorithm with a  $64\times 64$ -pixel interrogation window. The test results are given in Fig. 5, in which symbol  $f$  ( $=64$ ) represents the side length of the interrogation window. Test results in Fig.5a show that the evaluation error without filtering increases rapidly when the relative amplitude of the low frequency noise increases at  $A_{lf}/G_c > 0.5$ . When the high-pass filters are applied, the evaluation errors do not depend on the amplitude of the low frequency noise; i.e. the high-pass filters completely remove the influence of the low frequency noise. Fig.5b shows that the evaluation errors of the gradient filter and Laplace filter become very large when the single pixel random noise is added. The  $21\times 21$ -pixel unsharp mask has very good performance in both test cases, i.e. with and without random noises. The influence of the unsharp mask filter size on the evaluation accuracy is further investigated with two pairs of synthetic PIV recordings. One of them does not have any noise, whereas another has the single pixel random noise of  $G_{rms}/G_c=0.056$ . The particle image parameters are set as  $N_{tot}=10240$ ,  $G_0=90$ ,  $G_c=180$ , and  $D_p=3\sim 6$  pixels. The two synthetic PIV recording pairs are processed with the unsharp mask of different side lengths and then evaluated using the CCWS algorithm with a  $32\times 32$ -pixel interrogation window. The test results, including those without filtering, are given in Fig. 6. Fig.6 shows that the unsharp mask of small filter size (e.g.  $< 9$  pixels) may increase the evaluation error like the gradient filter and Laplace filter, but it has no side effects when the filter side length is not less than twice of the maximal particle image diameter, i.e.  $\geq 12$  pixels in this test case.

Fig. 6 shows that the unsharp mask of small filter size (e.g.  $< 9$  pixels) may increase the evaluation error like the gradient filter and Laplace filter, but it has no side effects when the filter side length is not less than twice of the maximal particle image diameter, i.e.  $\geq 12$  pixels in this test case.

### 3.3. $\mu$ PIV image filter

According to investigations in section 3.2, the  $3\times 3$ -pixel rectangular smooth filter can be used effectively to remove the single pixel random noise, whereas the unsharp mask is an ideal tool to remove the low frequency background noise. To simplify the filter operation and reduce potential rounding errors, a new digital filter that combines features of the two previous filters is constructed as

$$G'(x, y) = \frac{1}{9} \sum_{-1}^1 \sum_{-1}^1 G(x-i, y-j) - \frac{1}{(2r+1)(2r+1)} \sum_{-r}^r \sum_{-r}^r G(x-i, y-j). \quad (11)$$

When using Eq.(6), the filter coefficient is determined by

$$C(i, j) = \begin{cases} \frac{1}{9} - \frac{1}{(2r+1) \cdot (2r+1)} & \text{If } -1 \leq i \leq 1 \text{ and } -1 \leq j \leq 1 \\ \frac{1}{(2r+1) \cdot (2r+1)} & \text{otherwise} \end{cases} \quad (12)$$

The new filter is named the  $\mu$ PIV image filter, because it is designed to remove the strong single pixel random noise and low frequency noise from  $\mu$ PIV recordings. As indicated in Fig.6, the radius of the  $\mu$ PIV image filter ( $r$ ) should be larger than the maximal particle image diameter.

## 4. APPLICATION EXAMPLE

The  $\mu$ PIV image filter is applied in the PIV experiment of water flow in a deep microchannel, which has a rectangular cross-section of  $200\times 600 \mu\text{m}^2$  and a length of 120mm. The fluorescent polystyrene particles (Duke Scientific, Palo Alto, CA) used for the present experiment have a peak excitation wavelength of 542 nm and 612 nm for emission. The

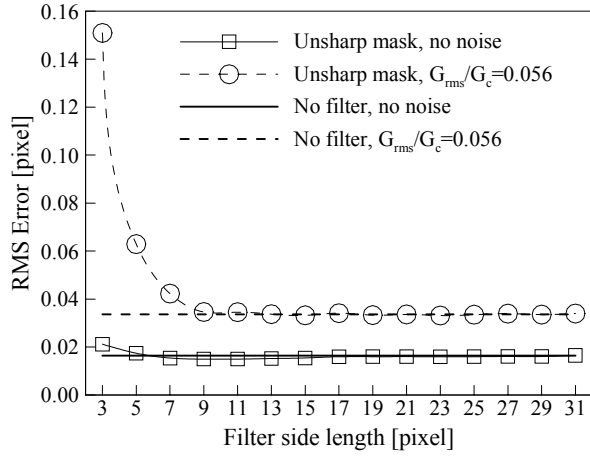


Fig.6: Evaluation error distributions on the filter side length of the unsharp mask

diameter and density of the particles are  $0.69\mu\text{m}$  and  $1050\text{ kg/m}^3$ , respectively. The pulsed laser beam is generated by a double cavity NewWave Nd:YAG laser, delivered into the inverted epi-fluorescent microscope (Nikon TE200) through the beam expander assembly, and guided to the flow field of the microchannel through a set of lenses inside the microscope and finally through a 20X microscope objective lens. The fluorescent particles suspended in the flow field absorb the illuminating light of  $\lambda=532\text{nm}$  (green) and emit light with a longer wavelength ( $\lambda\sim 612\text{nm}$ , red), which passes through the fluorescent filter cube into a Lavision Flowmaster 3S CCD camera of digital resolution of  $1024\times 1280$  pixels. The corresponding measurement area in the focal plane is  $348.3\times 435.4\ \mu\text{m}^2$ . Measurements are conducted at different positions along the channel with Reynolds number varying from hundreds to thousands to investigate transitions from laminar to turbulent flow in micro scale as well as the effect length scale and boundary conditions on entrance length. The time interval between laser pulses is carefully set so that the particle image displacements are around 10 pixels. 100 PIV recording pairs are taken for each case to enable use of the average correlation algorithm. A test is conducted downstream of the channel far from the entrance ( $67D_h$ ) at  $\text{Re}=1707$ . As shown in an evaluation sample pair in Fig. 7, the  $\mu\text{PIV}$  recordings have a strong single pixel random noise level ( $G_{rms}/G_c\approx 0.12$ ), and low frequency noises of different wavelengths can be observed easily, e.g. the dark spot in Fig.7 that probably results from some debris depositing on the glass cover of the microchannel. The averaged correlation function of 100 evaluation sample pairs at the same location as the pair of images shown in Fig. 7 are given in Fig.8a and 8b, respectively, for the cases with and without using  $\mu\text{PIV}$  image filter. Fig.8a shows that in the case without filtering the low frequency noise results in a dominant peak in the evaluation function at zero displacement. The correlation peak of the particle image displacement can not be identified in the presence of this noise peak. When the  $\mu\text{PIV}$  image filter is used to remove the low frequency noise, a clear peak of the particle image displacement is observed, see Fig.8b.

In order to quantify the effects of the  $\mu\text{PIV}$  image filter on the evaluation of real  $\mu\text{PIV}$  recordings, the  $\mu\text{PIV}$  recording pairs are evaluated by using CDIC and average correlation method with and without  $\mu\text{PIV}$  image filter, respectively. The axial velocity ( $U$ ) profile of the fully developed microchannel flow is determined by averaging data at 160 cross-section cuts and shown in Fig.9a. The distributions of the standard deviation ( $\sigma$ ) of the axial velocity are provided in Fig.9b. The test results show that a much lower precision error level can be achieved by using  $\mu\text{PIV}$  image filter. Note that the velocity is normalized with the maximum velocity ( $U_{max}$ ) and the coordinate with the channel width ( $H$ ).

## 5. SUMMARY AND CONCLUSIONS

The present work is aimed to reducing the measurement uncertainty of  $\mu\text{PIV}$  by using digital filters to remove background noise in digital PIV recordings. The performance of the rectangular smooth filter, gradient filter, Laplace filter and unsharp mask are tested with synthetically generated PIV recording pairs. Simulations show that the  $3\times 3$ -pixel gradient and Laplace filter are very sensitive to the single pixel random noise, so that they are suggested not to be used in processing  $\mu\text{PIV}$  recordings. The  $3\times 3$ -pixel rectangular smooth filter can be used effectively to remove the single pixel random noise, but larger smooth filter sizes are not suggested. When the filter size is large enough, the unsharp mask can be used to minimize the low frequency background noise without any noticeable side effects. A  $\mu\text{PIV}$  image filter that combines the capabilities of both the  $3\times 3$ -pixel smooth filter and the unsharp mask is constructed to enable high accuracy evaluation of  $\mu\text{PIV}$  recordings in a single processing step. This new  $\mu\text{PIV}$  digital filter was applied to a microchannel flow, demonstrating the performance of the new digital filter and confirming the simulation results. Although the analyses presented here are based on the correlation-based interrogation algorithms with continuous window shift, the conclusions can be extended to other processing techniques.

## ACKNOWLEDGEMENTS

This work was supported by the Indiana 21<sup>st</sup> Century Research and Technology Fund.

## REFERENCES

- Adrian RJ** (1991), Particle-Imaging Techniques for Experimental Fluid Mechanics. *Annu. Rev. Fluid Mech.* 23, 261-304
- Cenedese A; Paglialonga A** (1990), Digital direct analysis of a multiexposed photograph in PIV. *Exp. Fluids* 8,
- Fincham AM; Spedding GR** (1997), Low cost, high resolution DPIV for measurement of turbulent fluid flow. *Exp. Fluids* 23, 449-462
- Gui L** (1998) *Methodische Untersuchungen zur Auswertung von Aufnahmen der digitalen Particle Image Velocemetry.* Shaker Verlag, Aachen, Germany
- Gui L; Merzkirch W; Fei R** (2000) A digital mask technique for reducing the bias error of the correlation-based PIV interrogation algorithm, *Exp. Fluids* 29: 30-35
- Gui L.; Longo J; Stern F** (2001), Biases of PIV measurement of turbulent flow and the masked correlation-based interrogation algorithm. *Exp. Fluids* 30, pp. 27-35

- Gui L; Wereley ST** (2002) A correlation-based continuous window shift technique for reducing the peak locking effect in digital PIV image evaluation. *Exp. Fluids* 32: 506-517
- Heckmann W** (1996) *Auswertelgorithmen in der Particle Image Velocimetry*. Shaker Verlag, Aachen, Germany
- Heckmann W; Hilgers S; Merzkirch W; Schlüter T** (1994), Automatic Evaluation of Double-Exposed PIV Records by an Autocorrelation Method. *Optical Methods and Data Processing in Heat and Fluid Flow*, C485/021, City University, London, UK
- Huang HT; Fiedler HE; Wang JJ** (1993), Limitation and improvement of PIV — Part I: Limitation of conventional techniques due to deformation of particle image patterns. *Exp. Fluids* 15, 168-174
- Huang HT; Fiedler HE; Wang JJ** (1993), Limitation and improvement of PIV — Part II: Particle image distortion, a novel technique. *Exp. Fluids* 15, 263-273
- Keane RD; Adrian RJ** (1990), Optimization of particle image velocimeters. Part I: Double pulsed systems, *Meas. Sci. Technol.* 1, 1202-1215
- Kemmerich Th; Rath HJ** (1994), Multi-level convolution filtering technique for digital laser-speckle-velocimetry. *Exp. Fluids* 17, 315-322
- Lecordier B; Lecordier JC; Trinité M** (1999), Iterative sub-pixel algorithm for the cross-correlation PIV measurements. 3<sup>rd</sup> Int. Workshop on PIV, September 16-19, Santa Barbara
- Lecordier B; Demare D; Vervish LMJ; Réveillon J; Trinité M** (2001), Estimation of the accuracy of PIV treatment for turbulent flow studies by direct numerical simulation of multi-phase flow. *Meas. Science and Technology* 12: 1382-1391
- Lim JS** (1990) Two dimensional signal and image processing. PRENTICE HALL, Englewood Cliffs, New Jersey 07632
- Maas HG** (1992), *Digitale Photogrammetrie in der dreidimensionalen Strömungsmeßtechnik*, Diss. ETH Nr. 9665
- Meinhart CD, Wereley ST, Santiago JG** (1999) PIV measurements of a microchannel flow, *Exp. Fluids*, Vol. 27, 414-419
- Meinhart CD, Wereley ST, Santiago JG** (2000) A PIV algorithm for estimating time-averaged velocity fields, *Journal of Fluids Engineering*, Vol. 122, 285-289
- Meinhart CD and Zhang H** (2000) The flow structure inside a microfabricated inkjet printer head, *J. Microelectromechanical Systems*, Vol. 9, 67-75
- Okamoto K; Hassan YA; Schmidl WD** (1995), New tracking algorithm for particle image velocimetry. *Exp. Fluids* 19, 342-347
- Santiago JG, Wereley ST, Meinhart CD, Beebe DJ, Adrian RJ** 1998, A particle image velocimetry system for microfluidics. *Exp. Fluids* 25, 316-319
- Scarano F** (2002) Iterative image deformation methods in PIV. *Meas. Sci. Tech.* 13 (1): R1-R19 JAN 2002
- Sholl MJ; Savas Ö** (1997), A fast Lagrangian PIV method for study of general high gradient flow. 35<sup>th</sup> AIAA Aerospace Science Meeting, Reno, NV, Jan 6-9, AIAA paper 97-0493 (A97-15543)
- Sjödahl M** (1994), Electronic speckle photography: increased accuracy by nonintegral pixel shift. *Applied Optics* 33(28): 6667-6673
- Tokumaru PT; Dimotakis PT** (1995) Image correlation velocimetry. *Exp Fluids* 19: 1-15
- Wereley ST, Santiago JG, Meinhart CD, Adrian RJ** 1998, Velocimetry for MEMS Applications. *Proc. of ASME/DSC*, Vol. 66, (*Micro-fluidics Symposium*, November, Anaheim, CA)
- Wereley ST; Gui L; Meinhart CD** (2002) Advanced algorithms for microscale velocimetry. *AIAA Journal* Vol. 40, #6
- Wereley ST; Gui L** (2001) PIV measurement in a four-roll-mill flow with a central difference image correction (CDIC) method, 4th International Symposium on Particle Image Velocimetry, Göttingen, Germany, Sept. 17-19
- Wereley ST; Gui L** (2002) A correlation-based central difference image correction (CDIC) method and application in a four-roll-mill flow PIV measurement. *Exp. Fluids* (submitted)
- Westerweel J; Draad A; Hoesven J; Oord J** (1996), Measurement of fully-developed turbulent pipe flow with digital particle image velocimetry, *Exp. Fluids* 20, 165-177
- Westerweel J; Dabiri D; Gharib M** (1997), The effect of a discrete window offset on the accuracy of cross-correlation analysis of digital PIV recordings, *Exp. Fluids* 23, 20-28
- Willert CE** (1996), The fully digital evaluation of photographic PIV recordings. *Appl. Sci. Res.* 56, 79-102
- Willert CE; Gharib M** (1991), Digital Particle Image Velocimetry. *Exp. Fluids* 10, 181-193